9 Mg^+–X and Y–Mg^+–X Complexes Important in the Chemistry of Ionospheric Magnesium (X = H_2O, CO_2, N_2, O_2 and O)

9.1 Introduction

Magnesium is one of the most abundant metals in the mesosphere and lower thermosphere (MLT) region of the atmosphere. As with calcium (Chapter 8) the source of these metals is through the ablation of meteorites owing to frictional heating with ambient air molecules as they enter Earth's atmosphere. This deposition mechanism accounts for the addition of approximately six tons of magnesium per day[1] into the Earth's atmosphere resulting in the formation of a global layer of atomic magnesium between 80 and 110 km above the Earth's surface. Magnesium is also thought to be of importance in other atmospheres, such as Titan's in which it is also present.[2]

A schematic diagram summarizing the important reactions of the chemistry of magnesium in the MLT region is given in Figure 9.1. The foundation for this proposed ion-molecule chemistry derives from previous work on the sporadic layers of Ca (see Chapter 8 and reference 3), Na,[4] and K.[5]

Atomic Mg^+ ions have been detected in the mesosphere and lower thermosphere by rocket-borne mass spectrometry,[6,7,8] by photometric observations performed by rockets[9] and satellites,[10] and more recently

by the satellite-borne SCIAMACHY spectrometer measuring the dayglow in the limb.[11] However, detection of neutral atomic Mg in the upper atmosphere is limited to satellite-borne experiments.[11] This is owing to the fact that the Mg(3^1P_1 – 3^1S_0) transition at 285.2 nm is overlapped by the Huggins and Hartley bands of ozone,[1] making ground-based observations, by a technique such as LIDAR, impossible owing to the amount of ozone in the stratosphere.

The difficulty in experimentally moinitoring neutral atomic metals in the MLT region has led to chemical modelling of this region proving to be a powerful tool in the armoury of the atmospheric chemist. Quantum chemical calculations provide knowledge of energy levels from which rate coefficients, through (for example) the application of Rice-Ramsperger-Kassell-Marcus (RRKM) theory, can be determined. In the most useful cases, these are convolved with atmospheric parameters (partial pressures, electron densities and temperatures) to yield predicted concentration profiles, which can be compared with observations (both observational in the Earth's atmosphere,[12] and in the laboratory[13]). As well as work on Na,[4] K[5] and Ca (see Chapter 8 and reference 3) in which a similar approach to work herein has been taken, there have also been studies on Al,[14,15] Mg[15,16,17,18,] Fe[19] and Si.[16] A recent study[18] on magnesium has termed the $MgOH^+$ ion "pivotal", and indeed this ion was considered in early work.[20] However, this seems unlikely given the relatively low concentration of H_2O_2, which is required to form it through reaction with Mg^+. [H_2O_2] is predicted to be at least 2 orders of magnitude less than [O_3] above 70 km,[21] so that it is much more likely that Mg^+ will form molecular ions

via reactions with O_3 or *via* association reactions with X (X=N_2, O_2, CO_2, O or H_2O). In the present work, a similar set of calculations are performed to those described in Chapter 8 in which the chemistry of Ca was investigated in the MLT region of the atmosphere.

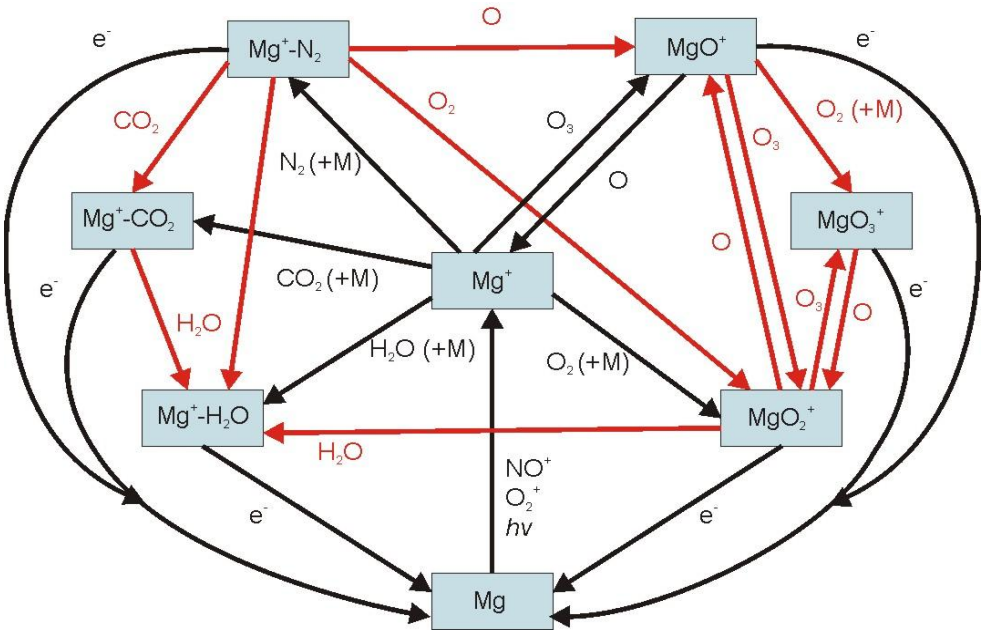

Figure 9.1. Schematic diagram of reactions important to the ion-molecule chemistry of Mg and Mg^+ in the MLT region of the atmosphere. The red arrows represent ligand switching reactions.

9.2 Computational details

Calculations were carried out on Mg^+–X and $[X–Mg–Y]^+$ intermediate ionic complexes using the GAUSSIAN 03 suite of programs,[22] in order to obtain accurate binding energies, harmonic vibrational frequencies, and rotational constants. In Chapter 8 and previous studies on similar systems[4,5] geometry optimizations were performed at both the B3LYP and MP2 levels of theory with little difference observed between the two methods. In these previous studies, owing to time and cost constraints, a complete set of subsequent higher-level single point

calculations were only obtained at geometries determined using the B3LYP method. Thus, in the present study, geometry optimization calculations have only been performed at the B3LYP level with Pople 6-311+G(2d,p) valence triple-ζ basis set. These B3LYP energies are used to calculate binding energies, D_e with the corresponding D_0 values are obtained by applying zero-point vibrational energy (ZPVE) corrections. In addition, UCCSD(T)/aug-cc-pVQZ single-point energy calculations at the B3LYP-optimized geometries were conducted using GAUSSIAN 03, in which only the valence electrons were correlated. Subsequent RCCSD(T) single-point calculations employed MOLPRO,[23] with the standard Dunning aug-cc-pVQZ basis sets being used for first row elements, while for Mg^+ the aug-cc-pCVQZ basis set was employed. In the RCCSD(T) calculations, only the Mg, N, C and O 1*s* orbitals were kept frozen, which is why a basis set for Mg^+ was selected which includes "tight" functions to describe the core-valence correlation. In both sets of CCSD(T) calculations, the B3LYP vibrational energies were employed to correct D_e to D_0 values. The complete basis set method (CBS-Q)[24] is a relatively cheap method which often produces surprisingly good energetics. The CBS-Q and UCCSD(T) bond energies for the Mg^+-X complexes were determined by Professor John Plane and co-workers at the University of Leeds but have been included in this study for comparison with the high-level RCCSD(T) results. The B3LYP calculated D_0' values and geometries for the Mg^+-X complexes were determined both as part of the current study and at the level at University of Leeds.

9.3 Ab initio calculations on Mg^+–X complexes

9.3.1 Mg^+–H_2O

There have been a number of studies reported on the Mg^+–H_2O complex (and higher complexes), and its fully deuterated isotopomer.[25,26,27,28,29,30,31,32,33] The first of these studies used photodissociation experiments to yield a very high D_0 value of 251 ± 20 kJ mol^{-1},[25] however, later studies using similar techniques yielded considerably lower values of 104 kJ mol^{-1} (reference 26) and 102 kJ mol^{-1} (reference 27). The optimized geometry obtained in the current study is shown in Figure 9.2a with the associated vibrational frequencies and rotational constants reported in Table 9.1. The obtained RCCSD(T) D_0 value of 130.8 kJ mol^{-1}, for the $\tilde{X}\,^2A_1$ state is somewhat higher than the later experimental values shown in Table 9.2, but is in excellent agreement with the B3LYP, UCCSD(T) and CBS-Q values (see Table 9.2). Other theoretical values have yielded values of 150 ± 20 kJ mol^{-1} (reference 34, also cited in reference 35) using the MCPF approach with fairly large basis sets, 130 kJ mol^{-1} using the CASSCF+MRCI approach,[36] 155 kJ mol^{-1} using the POLCI approach,[29] and 160 kJ mol^{-1} using the MP4 approach.[32] All of these values are higher than the more recent spectroscopic values,[26,27] but are lower than the earlier ones.[25] More recently, a value of 119 kJ mol^{-1} was obtained at the MP2/6-311+G(2d,2p) level by Andersen *et al.*,[37] with values of 119.6 and 121.7 kJ mol^{-1} being reported by Dunbar and Petrie[38] using both CP-MP2(thaw) and the CP-dG2thaw single-point calculations, respectively, at the B3LYP/6-311+G** optimized geometry. Given the higher level of theory employed herein,

and the agreement between the RCCSD(T), UCCSD(T), CBS-Q and B3LYP values, and other more recent values, it is likely that the theoretical binding energy value is the more reliable, and that the experimental value is in need of re-measurement.

It seems that there has only been one earlier report of vibrational frequencies, determined at the Hartree-Fock level,[36] where the ordering of the lowest two vibrational frequencies is different to that obtained here (see Table 9.1). Again, experimental measurement of these quantities is desirable.

9.3.2 Mg^+–N_2

In line with previous work on Ca^+–X (see Chapter 8), and electrostatic considerations[28] the present calculations confirmed, as expected, that N_2 prefers to bind end–on with Mg^+, giving a linear $^2\Sigma^+$ state (see Figure 9.2b); a result which is in line with previous theoretical results.[39,40] The obtained RCCSD(T) value of 30.1 kJ mol^{-1} is close to that obtained through B3LYP and UCCSD(T) (see Table 9.2). It is also in reasonable agreement with the CBS-Q calculation and the previous MRCI+Q value obtained by Maitre and Bauschlicher.[40] The derived D_0 value obtained in photodissociation experiments[41] was deemed unreliable therein, since the observed vibrational progression in the electronic spectrum was not thought to correspond to the $Mg^+\cdots N_2$ stretch. The vibrational frequencies are presented in Table 9.1, together with those obtained in reference 40 at both the MCPF and MRCI+Q levels of theory where good agreement is seen.

Table 9.1. Total energies, electronic states, harmonic vibrational frequencies and rotational constants of the Mg^+–X complexes obtained at the B3LYP/6-311+G(2d,p) level of theory.[a]

X	State	Total Energy (E_h)	Vibrational Frequencies (cm^{-1})	Rotational constants (GHz)
CO_2	$^2\Sigma^+$	-388.484007	61(π), 243(σ), 641(π), 1364(σ), 2433(σ)	0.00, 2.40, 2.40
H_2O	$^2A_1$	-276.320972	348(b_1), 381(a_1), 510(b_2), 1661(a_1), 3717(a_1), 3795(b_2)	412.82, 10.69, 10.42
			394(a_1), 460(b_1), 570(b_2), 1798(a_1), 4024(a_1), 4105(b_2)[b]	
N_2	$^2\Sigma^+$	-309.384456	130(π), 164(σ), 2443(σ)	0.00, 4.03, 4.03
			150(π), 178(σ), 2424(σ)[c]	
			148(π), 174(σ), 2390(σ)[d]	
O_3	$^2B_1$	-425.403527	261(b_1), 446(b_2), 477(a_1), 766.2(a_1), 872.2(b_2), 1065.9(a_1)	12.60, 8.35, 5.02
O	$^2\Pi$	-274.980294	*709*(σ)	0.00, 15.67, 15.67
			902[e]	
O_2	$^2A_2$	-350.204815	524 (b_2), 656 (a_1),1110 (a_1)	33.62, 11.83, 8.75

[a] Italicized values are from previous work — see the appropriate footnotes.

[b] Reference 36. SCF values, [c] Reference 40, MRCI+Q values,

[d] Reference 40, MCPF values [e] Reference 45 CISD value.

9.3.3 Mg^+–CO_2

Owing to previous studies on Ca^+ (see Chapter 8), and electrostatic arguments[28] only the end-on approach of CO_2 to Mg^+ was considered, yielding a $^2\Sigma^+$ state with the calculated geometry being shown in Figure 9.2c. The RCCSD(T) D_0 value (see Table 9.2) of 67.0 kJ mol^{-1} is in relatively good agreement with that of Willey *et al.*[42] who obtained the value of 62 kJ mol^{-1}. This value was determined indirectly from photodissociation experiments using the dissociation energy for the observed excited $^2\Pi$ state, derived from a (long) Birge-Sponer extrapolation, and the known associated atomic transition. There is a more-recent value of 58 ± 6 kJ mol^{-1} obtained by Andersen *et al.*[37]

using guided ion beam techniques, which is slightly lower than the present value, although in agreement (within experimental error) with the spectroscopic value.

Table 9.2. Dissociation energies (kJ mol^{-1}) of the Mg^+–X Complexes (X = H_2O, CO_2, N_2, O, O_2 and O_3). D_0 (D_e) values shown.

Level of theory	Species					
	Mg^+–H_2O	Mg^+–CO_2	Mg^+–N_2	MgO^+	MgO_3^+	MgO_2^+
B3LYP	130.6 (137.0)	61.7 (63.3)	28.2 (30.7)	208.3 (212.8)	269.2 (273.3)	50.9 (54.8)
CBS-Q[a]	126.9	64.1	35.6	224.3	263.1	90.1
UCCSD(T)[b]	127.4	63.8	28.3	217.6	266.0	89.0
RCCSD(T)[c]	130.8 (137.1)	67.0 (68.6)	30.1 (32.6)	216.2 (220.4)	261.4 (265.4)	90.0 (94.0)
Experimental	102[27]	62[42]		220±15[25] 110<D_0<170[47] 106<D_0<300[49] 240±10[50]		≤ 110[52]
Previous theoretical	150[34]	66[43] 61[38]	41[40]	224[44] 228[46]	118.5[18]	98[51] 36[46]

[a] Calculations performed at the University of Leeds

[b] UCCSD(T) calculations performed with GAUSSIAN 03. Only valence electrons were correlated. The aug-cc-pVQZ basis set was employed.

[c] RCCSD(T) calculations performed with MOLPRO. Only the 1*s* orbitals of Mg, N, C and O were frozen. The aug-cc-pCVQZ basis set was employed.

As can be seen in Table 9.2 there is very good agreement between the different levels of theory employed herein. A previous theoretical value of 66 kJ mol^{-1} by Sodupe *et al.*,[43] obtained at the MCPF level of theory with large basis sets, is also in excellent agreement with the present RCCSD(T) value, with a very similar geometry (see Figure 9.2c). No vibrational frequencies were reported in reference 43, with which to compare the current values listed in Table 9.1. A value of D_0 of 54 kJ mol^{-1} obtained at the MP2/6-311+G(2d,2p) level of theory in reference

37 seems somewhat low. The most recent values appears to be those of Dunbar and Petrie[38] using both CP-MP2(thaw) and the CP-dG2thaw single-point calculations at the B3LYP/6-311+G** optimized geometry: the values of 53.9 and 60.7 kJ mol^{-1}, respectively, are both a little below those obtained here and those obtained in reference 43. It seems that this quantity is somewhat basis set dependent, but given the consistency between the present values and that of reference 43, the present RCCSD(T) is likely to be the most reliable, hence the experimental values, and other theoretical values, are likely to be slightly low.

9.3.4 MgO^+

The ground state of Mg^+–O was found to be $^2\Pi$, in agreement with references 44 and 45, and may largely be described as Mg^{2+}–O^-. The bond length obtained is indicated in Figure 9.2d. The obtained RCCSD(T) binding energy of 216.2 kJ mol^{-1} is in very good agreement with the redetermined theoretical value[44] of 224 ± 6 kJ mol^{-1} (confirming the earlier value of 223 kJ mol^{-1}).[45] These values were calculated by Bauschlicher *et al.*, using both MCPF and CCSD(T) calculations in which only the 1*s* orbitals on all atoms were frozen, and employing augmented Dunning style basis sets of quadruple- and quintuple-ζ quality. In addition, there is very good agreement with the determined UCCSD(T) and CBS-Q values (Table 9.2), and an earlier CBS-Q calculation of 227.7 kJ mol^{-1} from Jursic,[46] however, the B3LYP value appears to be slightly low.

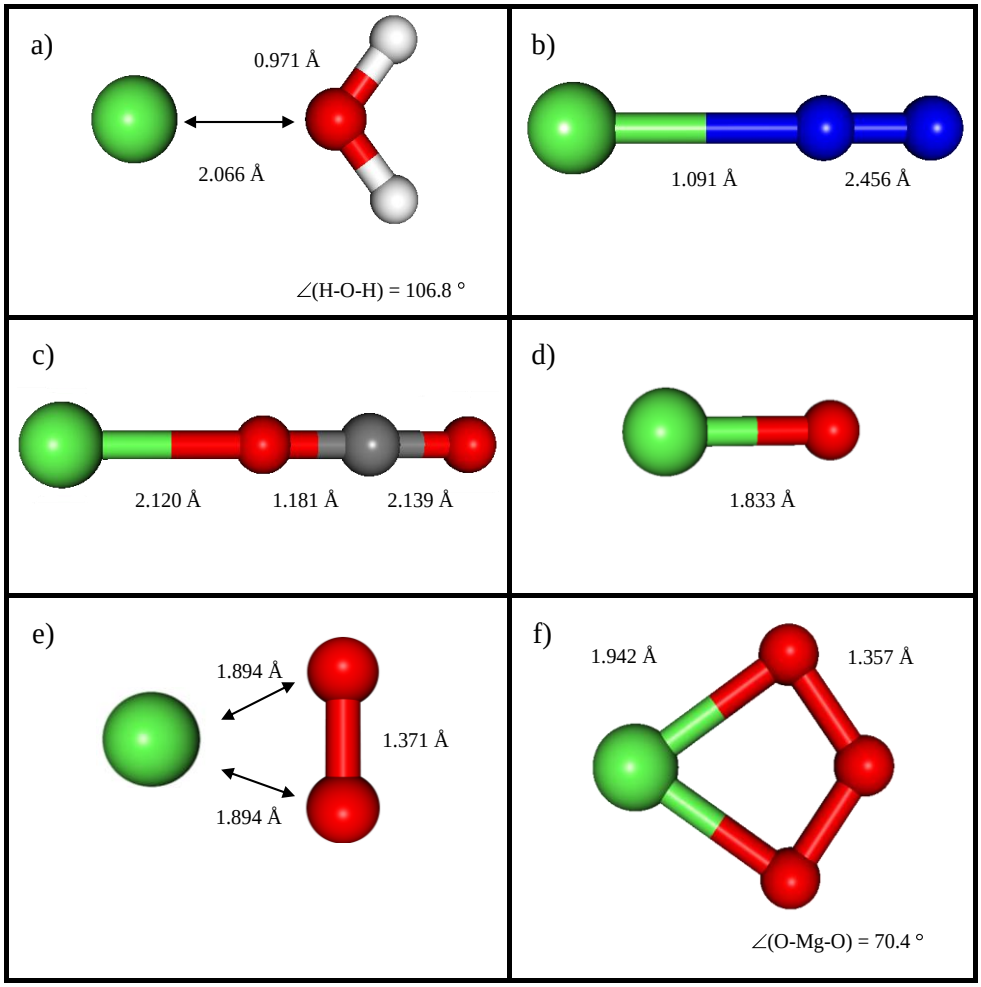

Figure 9.2. B3LYP/6-311G(2d,p) Optimized geometries of the Mg^+–X complexes. Note that the lines joining atoms do not necessarily indicate a chemical bond.

In addition there are a number of experimental values. The earliest appears to be from the ion cyclotron resonance (ICR) studies of Kappes and Staley,[47] who obtained a bracketed value, 110< D_0 < 170 kJ mol^{-1}, based on the fact that they were unable to observe MgO^+ when reacting Mg^+ with N_2O, but observed it in the reaction with O_3. This experimental result has been recently confirmed, showing that the reaction $Mg^+ + N_2O$ is very slow because there is a barrier of around 47 kJ mol^{-1} on the potential energy surface (PES).[48] Flowing afterglow studies reported by Rowe *et al.*[49] yielded a range of 106 < D_0 < 300 kJ mol^{-1}, which is consistent with the theoretical values, albeit that the

range is wide. Mass spectrometric experiments from Operti *et al.*[25] derived a value of D_0 = 220 ± 13 kJ mol^{-1}, which is in excellent agreement with the derived theoretical values. A subsequent determination of 240 ± 10 kJ mol^{-1} from guided-ion beam studies by Dalleska and Armentrout[50] on $Mg^+ + O_2$ was concluded as being slightly too high by Bauschlicher *et al.*,[44] in agreement with the current study.

9.3.5 MgO_2^+

Like N_2, it is possible for O_2 to bind either end or side-on, but in addition to this it has to be considered whether the complex has an overall doublet or quartet multiplicity state. The results of the present study are in accordance with previous calculations[51] which indicate the O_2 binds side-on, giving rise to an $\tilde{X}\,^2A_2$ state, the geometry of which is shown in Figure 9.2e. This doublet state occurs as a result of charge transfer from the Mg^+ to the O_2, effectively giving $Mg^{2+}O_2^-$, and is in line with previous conclusions reached for CaO_2^+ in Chapter 8. The obtained RCCSD(T) calculated dissociation energy of D_0 = 90 kJ mol^{-1} (Table 9.2) is in very good agreement with a previously-determined theoretical value of 97.5 kJ mol^{-1}, obtained using the MCPF approach and atomic natural orbitals,[51] and is also in line with photodissociation experiments,[52] which derived $D_0 \leq$ 110 kJ mol^{-1}. Interestingly, the B3LYP value is very much lower than the RCCSD(T) one, but there is good agreement between the present RCCSD(T), UCCSD(T) and the CBS-Q values. (Jursic[46] obtained a very low result of 35.6 kJ mol^{-1} using the CBS-Q method suggesting an error therein.)

The obtained vibrational frequencies (Table 9.1) appear to be the only ones reported to date.

9.3.6 MgO_3^+

The optimized geometry of the MgO_3^+ is of C_{2v} symmetry, $\tilde{X}\,^2B_1$ (see Figure 9.2f) and can again be described largely in terms of charge transfer, yielding Mg^{2+}–O_3^-. The RCCSD(T) binding energy obtained is D_0 = 261 kJ mol^{-1}, which is very similar to the B3LYP, UCCSD(T) and CBS-Q values (Table 9.2). There has been a previous report of the binding energy for MgO_3^+, yielding values of only 131.2 kJ mol^{-1} and 118.5 kJ mol^{-1} at the dG2thaw and CP-dG2thaw levels.[14] Noting the ionic nature of the MgO_x^+ species (x = 1–3), then the binding energies ought to be dominated by the difference in the ionization energies of Mg^+ and Mg^{2+}, as well as the electron affinity of O_x^-. The electron affinities for O, O_2 and O_3 are 1.461, 0.440 and 2.103 eV (141, 42 and 203 kJ mol^{-1}) respectively,[53] suggesting that the binding energy of MgO_3^+ should be the highest of the three species, as determined in the present study. The value reported in reference 14 is therefore concluded to be far too low. The vibrational frequencies are given in Table 9.1, unfortunately there do not appear to be any other values with which to compare. The CaO_3^+ binding energy, D_0 was also calculated for comparison, using the same methods as for MgO_3^+, and using the basis sets described in Chapter 8, giving a RCCSD(T) value of 354 kJ mol^{-1}, a value that is close to the B3LYP value of 378 kJ mol^{-1} reported by Broadley *et al.*[54]

9.4 Intermediate Y–Mg⁺–X complexes

9.4.1 Intermediate Complexes involving only closed-shell ligands

Figure 9.1 shows the potentially important ligand switching reactions which may occur in the MLT, as discussed in Chapter 1; for these reactions the $[X–Mg–Y]^+$ intermediates are important. There are three closed-shell ligands (N_2, CO_2 and H_2O) giving rise to three intermediate complexes in which the open-shell Mg^+ is solely complexed to closed-shell species. Owing to steric and electrostatic interactions it would initially be expected that the two species would approach from roughly opposite sides of the Mg^+, as seen for Ca^+ (see Chapter 8) but the manner in which they approach allows for a number of possible structures for each of the three intermediate complexes. As in the Ca^+ work, a few general assumptions were employed to reduce the number of calculations required in this body of work. The first assumption was that H_2O would approach the Mg^+ *via* the δ^- oxygen with the hydrogen atoms pointing away. CO_2 has the potential to approach either end-on, allowing one of the δ^- oxygen to interact with the Mg^+, or side-on allowing both oxygens to interact with Mg^+. In this investigation the side-on approach has not been considered in line with conclusions in the Ca^+ study in Chapter 8, and in line with electrostatic considerations.[28] Although N_2 is expected to bind end-on,[28] the weaker binding energy, and possible effects from the other ligand in the complex suggested that in this case the preferred approach was less clear and hence both orientations were investigated. In each case the complexes were given the freedom to optimize away from the higher symmetry.

Table 9.3. Total energies, electronic states and harmonic vibrational frequencies for X–Mg^+–Y (X, Y = CO_2, H_2O and N_2) complexes optimized and calculated at B3LYP/6-311+G(2d,p) level of theory. Rotational constants are given for the highlighted global minima only. sN_2 denotes side-on binding, otherwise the binding is end-on, whilst *i* indicates an imaginary frequency.

X	Y	State	Energy (E_h)	Vibrational frequencies (cm^{-1})	Rotational Constants (GHz)
CO_2	N_2	$^2A'$	-498.054913	37(a′), 59(a″), 74(a′), 110(a″), 113(a′), 170(a′), 237(a′), 644(a′), 645(a″), 1362(a′), 2427(a′), 2434(a′)	5.55, 1.22, 1.00
CO_2	N_2	$^2\Sigma^+$	-498.050773	10*i*(π), 10*i*(π), 49(σ), 50(π), 50(π), 71(π), 71(π), 206(σ), 643(π), 643(π), 1361(σ), 2427(σ), 2439(σ)	
CO_2	sN_2	$^2A_1$	-498.047426	59*i*(b_2), 10(a_1), 10(b_1), 11 0(b_2), 61(b_2), 62(b_1), 242(a_1), 641(b_2), 641(b_1), 1364(a_1), 2432(a_1), 2432(a_1)	
CO_2	H_2O	$^2A'$	-464.987829	60(a″), 64(a′), 96(a′), 154(a″), 194(a′), 330(a″), 374(a′), 512(a′), 647(a′), 647(a″), 1357(a′), 1657(a′), 2419(a′), 3734(a′), 3817(a′)	104.44, 2.13, 2.09
CO_2	H_2O	$^2A_1$	-464.979867	57*i*(b_2), 52*i*(b_1), 26(b_2), 26(b_1), 86(a_1), 305(b_1), 329(a_1), 457(b_2), 652(b_2), 652(b_1), 1355(a_1), 1648(a_1), 2410(a_1), 3706(a_1), 3793(b_2)	
H_2O	N_2	$^2A'$	-385.891153	63(a′), 99(a″), 101(a′), 137(a″), 154(a′), 346(a″), 373(a′), 519(a′), 1663(a′), 2425(a′), 3733(a′), 3812(a′)	12.05, 2.71, 2.21
H_2O	N_2	$^2A_1$	-385.887152	13(b_1), 13(b_2), 48(a_1), 77(b_2), 79(b_1), 334(b_1), 365(a_1), 493.9(b_2), 1657(a_1), 2438(a_1), 3716(a_1), 3797(b_2)	
H_2O	sN_2	$^2A_1$	-385.884382	54*i*(b_2), 45*i*(a_2), 12(a_1), 23.9(b_1), 24(b_2), 347(b_1), 382(a_1), 509(b_2), 1660(a_1), 2433(a_1), 3718(a_1), 3795(b_2)	

The optimized geometries are shown in Figure 9.3a–c, with the term symbols, vibrational frequencies and rotational constants given in Table 9.3. The approach of the individual ligands in the complexes, $[H_2O–Mg–N_2]^+$, $[H_2O–Mg–CO_2]^+$ and $[CO_2–Mg–N_2]^+$ is as expected with H_2O and CO_2 approaching end-on *via* an electronegative oxygen atom, and N_2 end-on as seen in $Mg^+–N_2$ and in all similar work involving Ca^+ (Chapter 8 and reference 3), K^+ [5] and Na^+.[4] However, it is the manner in which they approach with respect to one another that is surprising, as the preferred approach is from the same side of the Mg^+ cation, in contrast to the Ca^+ cases. Similar geometries have been seen previously, however, by Bauschlicher and coworkers for $[Mg(CO_2)_2]^+$ [43] and $[Mg(H_2O)_2]^+$,[35] with the latter also having been observed by Watanabe *et al.*[32] The total energies and harmonic vibrational frequencies of the two ligands approaching from opposite sides of Mg^+ are shown in Table 9.3, and as can be seen these geometries give imaginary vibrational frequencies or higher total energies than for the other orientations, confirming that these structures are either located at a saddle point or only a local minimum on the potential energy surfaces, respectively. Previous work by Bauschlicher *et al.*[35,43] in which the binding of ligands to different metal cations was investigated suggests that this difference is due to relatively low-lying ^2D states present within calcium. These low-lying ^2D states allow $sd\sigma$ hybridization which, in contrast to the sp^2 hybridization occurring in magnesium (evident in the population analysis), reduces the charge density equally on both sides of the metal cation therefore favouring linear structures and not the bent structures observed in the case of magnesium.

Another subtlety is that there appears to be interactions between the ligands, suggesting steric repulsion (see Figure 9.3a–c), but clearly the electronic stabilization from sp^2 hybridization outweighs this steric effect.

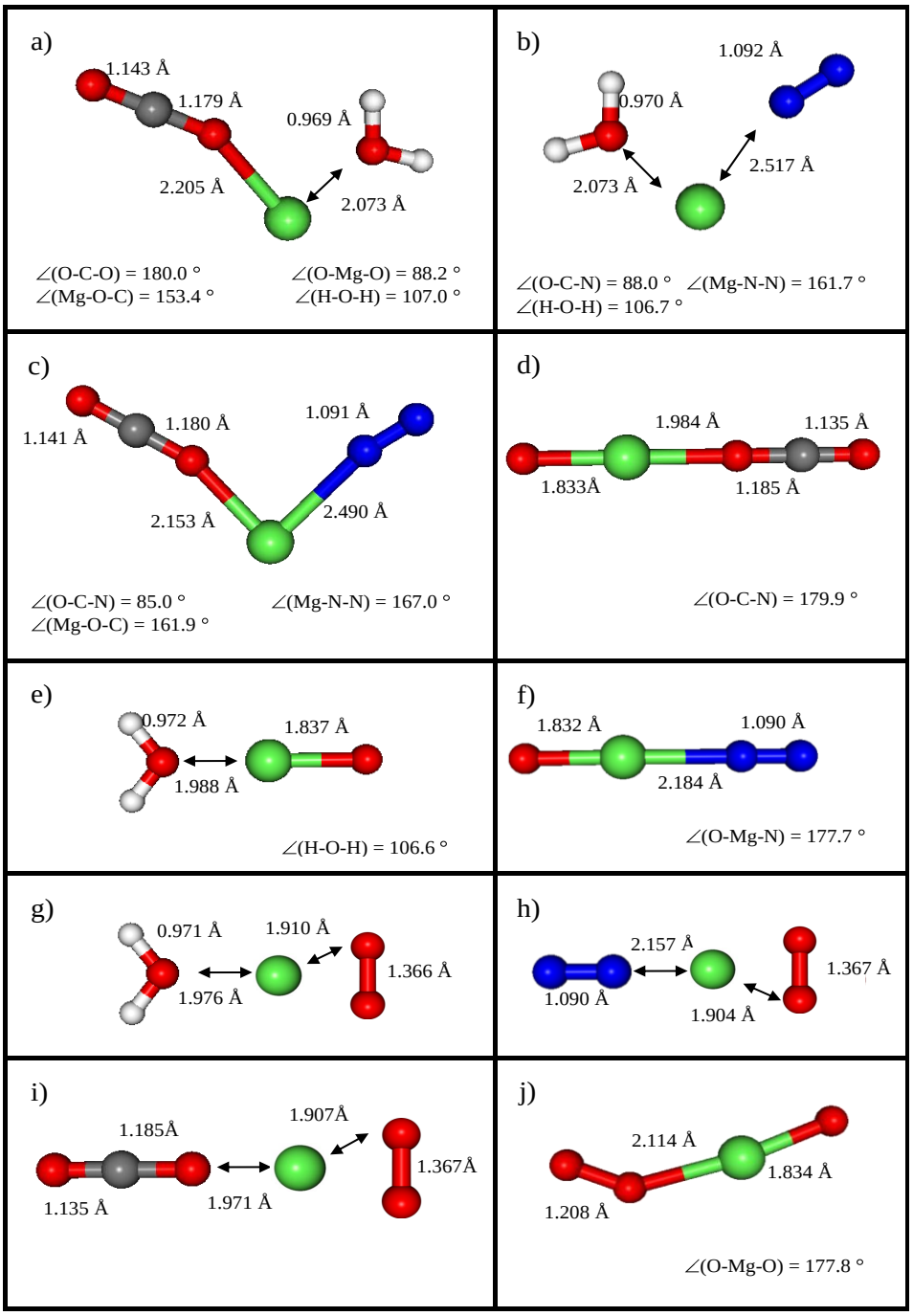

Figure 9.3. B3LYP/6-311+G(2d,p) optimized geometries of the $[X–Mg–Y]^+$ complexes. Note that the lines joining atoms do not necessarily indicate a chemical bond.

9.4.2 Geometries of $[O–Mg–X]^+$ intermediate complexes where (X= H_2O, CO_2 and N_2)

The oxygen atom has an open-shell ground state configuration (^3P) making the investigation of the $[O–Mg–X]^+$ complexes more involved than where the open-shell magnesium cation was complexed by two closed-shell ligands. In addition to a number of possible complexes with different orientations for each pair of ligands, there is the possibility that each complex could also have an either an overall quartet or doublet spin multiplicity. The doublet state arises from the formation of a chemical bond *via* charge transfer from the Mg^+ to the O, leaving a double positive charge on the magnesium and a single negative charge on the oxygen. In Chapter 8, work on the $[O–Ca–X]^+$ complexes indicated that charge transfer was present, hence the formation of a chemical bond occurring within $[O\text{-}Mg\text{-}X]^+$ complexes is likely. The calculated optimized structures for these complexes are shown in Figure 3d–f, with the vibrational frequencies and rotational constants given in Table 9.4. As can be seen, in contrast to where the Mg^+ is complexed to two closed shell ligands, all of the ligands approach in an essentially end-on manner from the opposite side to the oxygen atom. The rationale for this is that Mg is formally Mg^{2+}, and hence there is not the same opportunity for *sp* hybridization to occur. As a consequence, the ligands approach on opposite sides on steric grounds — this is in line with the conclusions of Bauschlicher and coworkers where dicationic complexes, such as $[Mg(H_2O)_2]^{2+}$, followed this mode of bonding.[37,45] As expected, in each case the doublet species was found to be lower in energy than the quartet species, consistent with the charge transfer from Mg^+ to O — this is

evinced by both the spin and charge analyses. It can also be seen (Table 9.4) that the end-on approach is preferred by N_2 regardless of whether the complex in question is in its quartet or doublet state, with only slight deviations away from linear approaches of this ligand.

Table 9.4. Total energies, electronic states and harmonic vibrational frequencies for O–Mg^+–X (X = CO_2, H_2O and N_2) complexes optimized and calculated at B3LYP/6-311+G(2d,p) level of theory. Rotational constants are given for the highlighted global minima only. sN_2 denotes side-on binding, otherwise the binding is end-on, whilst *i* indicates an imaginary frequency.

X	Y	State	Energy (E_h)	Vibrational frequencies (cm^{-1})	Rotational Constants (GHz)
N_2	O	$^2\Sigma^+$	-384.544895	49(π), 49(π), 222(π), 222(π), 288(σ), 830 (σ), 2453 (σ)	
N_2	O	$^4\Sigma^-$	-384.483339	24*i*(π), 24*i*(π), 93(σ), 104(π), 104(π), 148(σ), 2441(σ)	
N_2	O	$^2A'$	-384.578277	46(a′), 208(a″), 208(a″), 266(a″), 742(a′), 2452(a′)	15940.69, 2.12, 2.12
N_2	O	$^4A''$	-384.486000	49(a′), 110(a″), 123(a″), 136(a″), 197(a′), 2438(a′)	
sN_2	O	$^2A_1$	-384.520211	232*i*(b_2), 50(b_1), 53(b_2), 201(a_1), 824(a_1), 2384(a_1)	
sN_2	O	$^4A_2$	-384.476981	88*i*(b_2), 10*i*(b_1), *i*10(b_2), 22(a_1), 192(a_1), 2430(a_1)	
CO_2	O	$^2\Sigma^+$	-463.649500	43(π), 43(π), 116(π), 116(π), 314(σ), 631(π), 631(π), 831(σ), 1386(σ), 2461(σ)	
CO_2	O	$^4\Sigma^+$	-463.580734	22*i*(π), 22*i*(π), 46(π), 46(π), 107(σ), 198(σ), 644(π), 644(π), 1360(σ), 2424(σ)	
CO_2	O	$^2A''$	-463.682310	31(a′), 84(a″), 109(a′), 296(a′), 633(a′), 633(a″), 750(a′), 1382(a′), 2457(a′)	118080.85, 1.29, 1.29
CO_2	O	$^4A''$	-463.584191	49(a′), 59(a″), 77(a′), 181(a′), 223(a′), 644(a″), 645(a′), 1359(a′), 2425(a′)	
H_2O	O	$^2A''$	-351.522120	64(a′), 73(a″), 413(a′), 418(a″), 606(a′), 759(a′), 1682(a′), 3724(a′), 3784(a′)	408.32, 3.91, 3.87
H_2O	O	^4A	-351.419850	40(a), 58(a), 171(a), 353(a), 357(a), 495(a), 1659(a), 3718(a), 3798(a)	
H_2O	O	$^2B_1$	-351.522114	60(b_2), 73(b_1), 412(a_1), 420(b_1), 608(b_2), 758(a_1), 1682(a_1), 3721(a_1), 3781(b_2)	
H_2O	O	$^4A_2$	-351.416611	23*i*(b_2), 23*i*(b_1), 104(a_1), 325(b_1), 355(a_1), 480(b_2), 1654 (a_1), 3715(a_1), 3798(b_2)	

9.4.3 Geometries of $[O_2–Mg–X]^+$ intermediate complexes (X = H_2O, CO_2 and N_2)

O_2 is open-shell in its ground state ($X^3\Sigma_g^-$), so similar considerations as those for $[O–Mg–X]^+$ are required; in addition, O_2 like N_2 could bind both end- and side-on. Calculations on the MgO_2^+ species and similar studies on the $[O_2–Ca–X]^+$ intermediate complexes (see Chapter 8) indicate that the side-on approach is preferred by the O_2 ligand. The MgO_2^+ complex also exhibits charge transfer essentially giving Mg^{2+} and O_2^-, hence it is expected a similar situation will arise for the $[O_2–Mg–X]^+$ complexes. For this case the favoured approach of the second ligand will be "end-on" and from the opposite side to that of O_2, owing to the lack of *sp* hybridization on the Mg^{2+} centre, as for the $[O–Mg–X]^+$ species. Both side and end-on approaches, for both quartet and doublet multiplicity, were investigated for completeness.

Figure 9.3g–i shows the optimized geometry of each $[O_2–Mg–X]^+$ global minimum, with the harmonic vibrational frequencies and rotational constants given in Table 9.5. As expected, in each case the lowest energy complex is achieved when O_2 approaches side-on, while the other ligand approaches end-on from the opposite side to that of O_2, resulting in a doublet (not quartet) spin state, consistent with charge transfer from Mg^+ to O_2 occurring. The spin and charge analyses confirm that the unpaired electron is distributed equally over the two oxygen atoms. Examination of Table 9.5 interestingly also shows that when O_2 approaches in an end-on manner it is the quartet state that is energetically favourable in contrast to the doublet, shown by

imaginary frequencies calculated for the doublet state in this mode of approach.

Table 9.5. Total energies, electronic states and harmonic vibrational frequencies for O_2–Mg^+–X (X = CO_2, H_2O and N_2) complexes optimized and calculated at B3LYP/6-311+G(2d,p) level of theory. Rotational constants are given for the highlighted global minima only. sO_2 denotes side-on binding, otherwise the binding is end-on, whilst *i* indicates an imaginary frequency.

X	Y	State	Energy (E_h)	Vibrational frequencies (cm^{-1})	Rotational Constants (GHz)
CO_2	O_2	$^2\Sigma^+$	-538.860325	66*i*(π), 66*i*(π), 10(π), 10(π), 37(σ), 57(π), 57(π), 229(σ), 641(π), 641(π), 1363(σ), 1631(σ), 2430(σ)	
CO_2	O_2	$^4\Sigma^-$	-538.860751	9(π), 9(π), 43(σ), 54(π), 54(π), 65(π), 65(π), 222(σ), 642(π), 642(π), 1362.4(σ), 1626(σ), 2429(σ)	
CO_2	sO_2	$^2A_2$	-538.910676	33(b_1), 39(b_2), 105(b_1), 106(b_2), 274(a_1), 508(b_2), 631(b_2), 632(b_1), 679(a_1), 1125(a_1), 1386(a_1), 2460(a_1)	33.83, 0.99, 0.96
CO_2	sO_2	$^4B_1$	-538.859346	39*i*(b_2), 11(b_1), 13(b_2), 27(a_1), 60(b_2), 60(b_1), 236(a_1), 641(b_1), 641(b_2), 1364(a_1), 1619(a_1) , 2431(a_1)	
H_2O	O_2	$^2A_2$	-426.697062	53*i*(b_2), 51*i*(b_1), 23(b_2), 25(b_1), 37.0 (a_1), 342(b_1), 375(a_1), 503(b_2), 1631(a_1), 1659(a_1), 3717(a_1), 3796(b_2)	
H_2O	O_2	$^4A_2$	-426.697422	21(b_2), 23(b_1), 42(a_1), 70(b_2), 73(b_1), 340(b_1), 372 (a_1), 501(b_2), 1628(a_1), 1659(a_1), 3717(a_1), 3797(b_2)	
H_2O	sO_2	$^2A_2$	-426.750992	54(b_2), 69(b_1), 89(a_2), 387(a_1), 407(b_1), 505(b_2), 614(b_2), 698(a_1), 1126(a_1), 1681(a_1), 3725(a_1), 3785(b_2)	31.30, 2.94, 2.69
H_2O	sO_2	$^4A_2$	-426.642722	60(b_2), 69(a_2), 73(b_1), 293(b_2), 357(a_1), 418(b_1), 552(a_1), 608(b_2), 705(a_1), 1682(a_1), 3723(a_1), 3782(b_2),	
H_2O	sO_2	^2A	-426.750992	53(a), 68(a), 86(a), 387(a), 410(a), 505(a), 614(a), 699(a), 1127(a), 1682(a), 3725(a), 3784(a)	
H_2O	sO_2	$^4A''$	-426.699105	35(a′), 46(a″), 55(a′), 70(a′), 133(a″),	

				335(a″), 383(a′), 510(a′), 1628(a′), 165(a′), 3725(a′), 3805(a′)	
N_2	O_2	$^2\Sigma^+$	-459.761418	94*i*(π), 94*i*(π), 7*i*(π), 7*i* (π), 46(σ), 115(π), 115(π), 134(σ), 1632(σ), 2442(σ)	
N_2	O_2	$^4\Sigma^-$	-459.762151	12*i*(π), 12*i*(π), 55(σ), 73(π), 73(π), 106(π), 106(π), 118(σ), 1624(σ), 2442(σ)	
N_2	sO_2	$^2A_2$	-459.806721	34(b_1), 45(b_2), 214(b_1), 216(b_2), 260(a_1), 514(b_2), 666(a_1), 1121(a_1), 2453(a_1)	33.83, 1.63, 1.56
N_2	sO_2	$^4A_1$	-459.760097	52*i* (b_2), 4(b_1), 12(b_2), 38(a_1), 125(b_2), 126(b_1), 152(a_1), 1615(a_1), 2443(a_1)	
N_2	O_2	$^4A''$	-459.764048	32(a′), 64(a″), 68(a′), 94(a′), 118(a″), 121(a′), 163(a′), 1620(a′), 2441(a′)	
sN_2	O_2	$^2A''$	-459.777320	48(a′), 85(a″), 165(a″), 170(a′), 216(a′), 248(a′), 373(a′), 1266(a′), 2443(a′)	
sN_2	O_2	$^4A_2$	-459.755091	92*i* (b_2), 1*i*(b_1), 4(b_2), 22(a_1), 90(b_2), 92(b_1), 129(a_1), 1620(a_1), 2428(a_1)	
N_2	O_2	$^2A''$	-459.777320	48(a′), 85(a″), 165(a″), 169(a′), 216(a′), 248(a′), 374(a′), 1266(a′), 2444(a′)	

9.4.4 Geometry of O–Mg^+–O_2 intermediate complex

Of all the complexes studied in this body of work the intermediate complex ion composed of the three open-shell O_2, O, Mg^+ species was the most difficult, owing to the possibility of doublet, quartet and sextet spin states in addition to a selection of different structures. Calculations were performed for O_2 approaching the strongly bound MgO^+ moiety both end- and side-on, and for O approaching the strongly bound MgO_2^+ on both the same and opposite sides as O_2. Owing to the lowest excited singlet state of O atoms (^1D) and of O_2 ($^1\Delta_g$) being significantly higher in energy than the triplet states the doublet

and sextet states should not arise in geometries where the ligands are on opposite sides of Mg^+ with the quartet states are expected (from the combination of $MgO^+ + O_2$ and $MgO_2^+ + O$) however, for completeness these states were investigated. For the cases where all O atoms are on the same side of the complex, doublet or quartet states could arise.

Table 9.6 shows the results of these calculations and the lowest energy structure, as observed for Ca^+ (Chapter 8), is found to be the doublet ozonide structure, which is shown in Figure 9.2f. For the approach of the species from opposite sides of the magnesium cation, both linear structures, where O_2 was bound end-on, and structures in which O_2 was bound side-on (giving C_{2v} symmetry) were found to be located at saddle points on the potential energy surface. Hence unconstrained searches were undertaken yielding a C_1 (^4A) structure the geometry of which is shown in Figure 9.3j.

Table 9.6. Total energies, electronic states and harmonic vibrational frequencies for O_2–Mg^+–O complexes optimized and calculated at B3LYP/6-311+G(2d,p) level of theory. Rotational constants are given for the highlighted global minima only. sO_2 denotes side-on binding, otherwise the binding is end-on, whilst *i* indicates an imaginary frequency.

X	Y	State	Energy (E_h)	Vibrational frequencies (cm^{-1})	Rotational Constants (GHz)
O	O_2	$^2\Sigma^+$	-425.345295	62*i*(π), 62*i*(π), 53(π), 53(π), 272(σ), 829(σ), 1658(σ)	
O	O_2	$^4\Sigma^-$	-425.379874	73*i*(π), 69*i*(π), 37(π), 39(π), 245(σ), 736(σ), 1648(σ)	
O	O_2	$^6\Sigma^+$	-425.292034	14*i* (π), 14(π), 72(σ), 89(π), 89(π), 166(σ), 1621(σ)	
O	sO_2	$^2A_2$	-425.351319	236*i*(b_2), 34(b_1), 38(b_2), 175(a_1), 728(a_1), 1568(a_1)	
O	sO_2	$^4A_1$	-425.368037	220*i*(b_2), 33(b_1), 41(b_2), 127(a_1), 695(a_1), 1511(a_1)	
O	sO_2	$^6B_2$	-425.289275	62*i*(b_2), 13*i*(b_1), 8*i*(b_2), 46(a_1), 187(a_1), 1612(a_1)	
O	O_2	$^2A'$	-425.380252	36(a′), 66(a″), 115(a′), 254(a′), 736(a′), 1625(a′)	
O	O_2	$^4A'$	-425.380551	48(a′), 65(a″), 130(a′), 258(a′), 731(a′), 1611(a′)	104.44, 2.13, 2.09
O	O_2	$^6a'$	-425.293308	31(a′), 69(a′), 78(a″), 97(a′), 187(a′), 1619(a′)	
O	sO_2	$^2a'$	-425.380243	48(a′), 70(a″), 122(a′), 256(a′), 737(a′), 1625(a′)	
O	sO_2	$^4A'$	-425.368046	224*i*(a′), 31(a″), 42(a′), 135(a′), 704(a′), 1523(a′)	
O	sO_2	$^6A'$	-425.292065	12(a′), 74(a′), 83(a′), 87(a″), 166(a′), 1621(a′)	
O_2	O	$^2a''$	-425.362672	49(a″), 131(a′), 247(a′), 529(a′), 739(a′), 1475(a′)	
O_2	O	$^4A'$	-425.355821	20(a″), 22(a′), 44(a′), 53(a′), 704(a′), 1578(a′)	
O_2	O	$^6A'$	-425.293307	31(a′), 67(a′), 76(a″), 96(a′), 187(a′), 1619(a′)	
O	O_2	$^2B_1$	-425.403527	261(b_1), 446(b_2), 476(a_1), 766(a_1), 872(b_2), 1066(a_1)	
O	O_2	$^4B_1$	-425.295366	28*i*(b_2), 42(a_1), 61(b_1), 521(b_2), 654(a_1), 1110(a_1)	
O	O_2	$^6a_1$	-425.276391	95*i*(b_2), 12*i*(b_1), 15(a_1), 20(b_2), 81(a_1), 1601(a_1)	

9.4.5 Geometries of $Mg^+(X)_2$ complexes (X = H_2O, CO_2, N_2 and O_2)

In addition to ligand-switching reactions occurring between two different ligands, addition of the same ligand can initiate cluster formation. Thus, geometry optimizations and harmonic frequency calculations were carried out on $[X–Mg–X]^+$ complexes. Complexes in which the two ligands approached from opposite sides of Mg^+ were confirmed as being located at saddle points, as can be seen from the imaginary frequencies in Table 9.7. Relaxation of the symmetry restraints allowed the complexes to approach the Mg^+ from the same side resulting in the minimum geometries that are shown in Figure 9.4a,b, in agreement with conclusions[32,35,43] from previous studies with $[Mg(CO_2)_2]^+$ being of C_{2v} symmetry, and $[Mg(H_2O)_2]^+$ being of C_2 symmetry — see Figure 9.4. A number of structures were calculated for $[Mg(N_2)_2]^+$ with again a bent structure being the global minimum, giving a C_{2v} structure (Figure 9.4c). These "bent" structures are in contrast to the linear structures observed in the corresponding $[Ca(X)_2]^+$ complexes (see Chapter 8) and as mentioned above are thought to be due to relatively low-lying ^2D states in calcium allowing $sd\sigma$ hybridization,[35,43] which reduces charge density equally on both sides of the metal cation, favouring the linear structure. Another way of viewing this is that in $[Mg(X)_2]^+$ *sp* hybridization occurs on complexation of the first H_2O, creating a region of high electron density on the side opposite the first water, explaining why the second water approaches from the same side as the first.

Calculations examining the $[Mg(O_2)_2]^+$ complex, like the calculations described above on $[O–Mg–O_2]^+$, were carried out on a number of

structures which in turn were calculated with doublet, quartet and sextet multiplicity. As can be seen in Table 9.7, the global minimum was the $^4A'$ complex shown in Figure 4d. Similarities can be seen between this structure and the one calculated for O—Mg^+—O_2 in which the two ligands approached from different sides, as in both cases the approaching O_2 ligand is slightly bent away from the central axis.

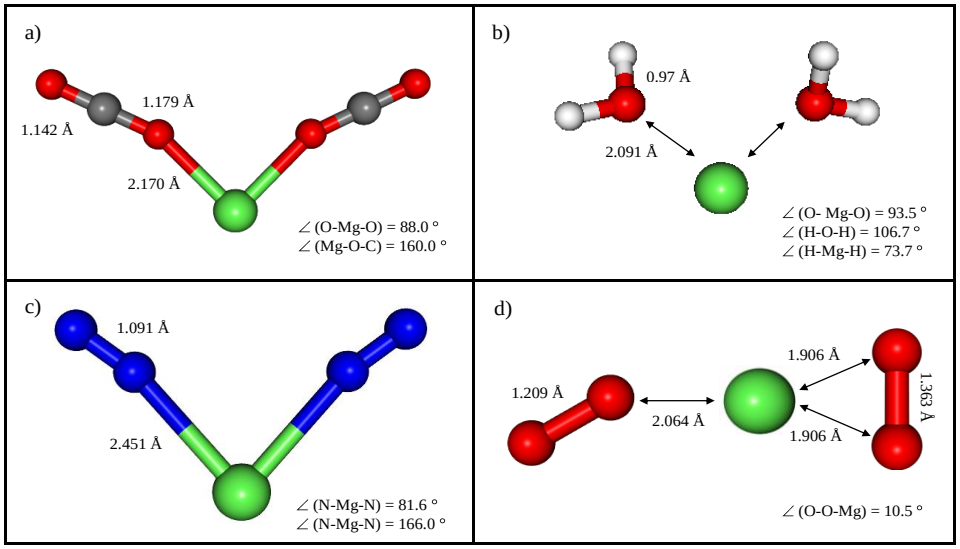

Figure 9.4. B3LYP/6-311+G(2d,p) optimized geometries of $[MgX_2]^+$ complexes. Note that the lines joining the atoms do not necessarily indicate a chemical bond.

Table 9.7 Total energies, electronic states and harmonic vibrational frequencies for X–Mg^+–X (X = O_2, CO_2, H_2O and N_2) complexes optimized and calculated at B3LYP/6-311+G(2d,p) level of theory. Rotational constants are given for the highlighted global minima only. sO_2 and sN_2 denotes side-on binding, otherwise the binding is end-on, whilst *i* indicates an imaginary frequency.

Complex	State	Energy (E_h)	Vibrational frequencies (cm^{-1})	Rotational Constants / GHz
CO_2–Mg^+–CO_2	$^2A_1$	-577.151644	30(a_1), 49(b_1), 57(a_2), 58(a_1), 89(a_1), 212(b_2), 233(a_1), 643(b_2), 645(a_1), 645(a_2), 646(b_1), 1361(b_2), 1363(a_1), 2416(b_2), 2433(a_1),	5.19, 0.78, 0.68
CO_2–Mg^+–CO_2	$^2\Sigma_g^+$	-577.144928	45*i*(π_u), 45*i*(π_u), 19(π_u), 19(π_u), 31(π_g), 31(π_g), 97(σ_g), 151(σ_u), 647(π_g), 647(π_g) 648(π_u), 648(π_u), 1356(σ_u), 1357(σ_g), 2411(σ_u), 2419(σ_g),	
H_2O–Mg^+–H_2O	^2A	-352.822190	67(a), 87(a), 208(a), 335(a), 342(a), 356(a), 364(a), 472(a), 523(a), 1652(a), 1657(a), 3724(a), 3725(a), 3808(a), 3808(a)	15.26, 5.50, 4.10
H_2O–Mg^+–H_2O	^2A_g	-352.813540	84*i*(b_{2u}), 68*i* (b_{3u}), 52*i*(a_u), 234(a_g), 276(b_{2g}), 281(b_{3u}), 370(b_{1u}), 395(b_{2u}), 443(b_{3g}), 1637(b_{1gu}), 1638(a_g), 3693(b_{1u}), 3693(a_g), 3786(b_{3g}) 3786(b_{2u}).	
N_2–Mg^+–N_2	$^2A_1$	-418.957375	50(a_1), 114(b_1), 116(a_1), 123(b_2), 128(a_2), 155(b_2), 213(a_1), 2433(a_1), 2435(b_2),	5.88, 2.08, 1.54
N_2–Mg^+–N_2	$^2\Sigma_g^+$	-418.953181	21*i*(π), 21*i*(π), 81(σ), 82.9(σ), 93(π), 93(π), 94(π), 94(π), 2440(σ), 2441(σ)	
sN_2–Mg^+–N_2	$^2A_1$	-418.947964	76.9*i* (b_2), 10.7 (b_2), 10.8 (b_1), 17.9 (a_1), 128.8 (b_2), 129.2 (b_1), 160.1 (a_1), 2430.2 (a_1), 2443.2 (a_1)	
sN_2–Mg^+–sN_2	^2A_g	-418.937588	125*i*(b_{2u}), 121*i*(b_{3g}), 12*i*(b_{3u}), 6*i*(a_u), 11(b_{2u}), 35(a_g), 51(b_{1u}), 2422(b_{1u}), 2422(a_g)	
sO_2–Mg^+–O_2	$^2B_2$	-500.549672	183*i*(b_1), 112*i*(b_2), 5*i*(b_1),	

			3(b_2), 27(a_1), 83(b_2), 113(a_1), 1621(a_1), 1621(a_1)	
sO_2–Mg^+–sO_2	^2A_g	-500.452940	161*i*(b_{2u}), 142*i*(b_{3g}), 18*i*(b_{3u}), 9(a_u), 24(b_{2u}), 85(a_g), 119(b_{1u}), 1595(b_{1u}), 1596(a_g)	
O_2–Mg^+–O_2	$^4A'$	-500.608190	22(a″), 40(a'), 55(a″), 108(a′), 244(a′), 505(a′), 594(a′), 1098(a′), 1573(a′)	29.60, 1.58, 1.50
O_2–Mg^+–O_2	$^4\Sigma_g^-$	-500.567983	132*i*(π), 132*i*(π), 130*i*(π), 130*i*(π), 11*i*(π), 11*i* (π), 60(σ), 60(σ), 1629(σ), 1629(σ)	
sO_2–Mg^+–O_2	$^4A_1$	-500.607931	65*i*(b_1), 52*i*(b_1), 36(b_1), 50(b_2), 241(a_1), 504(b_2), 594(a_1), 1102(a_1), 1595(a_1)	
sO_2–Mg^+–sO_2	^4A_g	-500.561097	155*i*(b_{2u}), 149*i*(b_{3g}), 11*i*(b_{3u}), 16(b_{2u}), 18(a_u), 34(a_g), 54(b_{1u}), 1615(b_{1u}), 1616(a_g)	
O_2–Mg^+–O_2	$^6A_1$	-500.571144	22(a_1), 56(b_2), 63(a_2), 68(b_1), 69(a_1), 93(b_2), 119(a_1), 1620(b_2), 1621(a_1)	
O_2–Mg^+–O_2	$^6\Sigma_g^+$	-500.570254	11*i*(π), 11*i*(π), 70(σ), 71(π), 71(π), 81(σ), 82(π), 82(π), 1620(σ), 1621(σ)	
sO_2–Mg^+–O_2	$^6A_1$	-500.500029	85*i*(b_2), 70*i*(b_1), 43(b_1), 60(b_2), 229(a_1), 284(b_2), 504(a_1), 688(a_1), 1656(a_1)	
sO_2–Mg^+–sO_2	^6A_g	-500.563112	88*i*(b_{2u}), 79*i*(b_{3g}), 18*i*(b_{3u}), 22(b_{2u}), 23(a_u), 51(a_g), 79(b_{1u}), 1604(b_{1u}), 1604.6 (a_g)	

9.4.6 RCCSD(T) calculations

Accurate total energies are required for elucidating possible reactions pathways, as well as reliably applying statistical theories such as RRKM to obtain rate coefficients for reactions occurring in the upper atmosphere (Figure 9.1).[3,4,5] Hence, single point energy RCCSD(T) calculations were performed at the B3LYP/6-311+G(2d,p) optimized geometries using the aug-cc-pCVQZ basis set for magnesium, allowing the inclusion of the inner valence electrons of Mg^+ in the correlation

treatment, allowing further recovery of dynamic correlation energy. In Table 9.8, the RCCSD(T) energies calculated are presented from which the binding energies in Table 9.9 are derived; in addition, the B3LYP binding energies are shown. The general behaviour of the B3LYP *versus* RCCSD(T) binding energies, is very similar to that observed in Table 9.2 for removal of the corresponding ligand.

Table 9.8. RCCSD(T) Total Energies

Species	Total Energy (E_h)
CO_2	-188.389569
H_2O	-76.363532
O	-74.994931
O_2	-150.177984
N_2	-109.407028
Mg^+	-199.675055
CO_2	-388.09077
H_2O	-276.090811
N_2	-309.094512
O	-274.750982
sO_2	-349.888824
$H_2O—Mg^+— CO_2$	-464.500076
$N_2—Mg^+—CO_2$	-497.507368
$N_2—Mg^+—H_2O$	-385.506604
$N_2—Mg^+—O_2$	-459.334294
$N_2—Mg^+—O$	-384.197470
$O_2—Mg^+—H_2O$	-426.337227
$O—Mg^+—CO_2$	-463.197985
$O—Mg^+—H_2O$	-351.199964
$O_2—Mg^+—CO_2$	-538.334632
$O_2—Mg^+—O$	-424.958359
$N_2—Mg^+—N_2$	-418.513185
$O_2—Mg^+—O_2$	-500.094642
$CO_2—Mg^+—CO_2$	---[a]
$H_2O—Mg^+—H_2O$	-352.497574

[a] exceeds resources

Previous theoretical binding energies are only available for $[Mg(H_2O)_2]^+$ and $[Mg(CO_2)_2]^+$; in the case of $[Mg(H_2O)_2]^+$ the obtained RCCSD(T) D_e

value of 113.5 kJmol^{-1} compares well to that of 109.6 kJ mol^{-1} obtained using the MCPF approach with a fairly large basis set,[34] and 112.1 kJmol^{-1} using the MP4 approach.[32] It may also be seen that the B3LYP value obtained herein is in excellent agreement with those obtained at the higher levels of theory. For $[Mg(CO_2)_2]^+$, our B3LYP D_e value of 44.6 kJ mol^{-1} is in excellent agreement with the value of 46 kJ mol^{-1} obtained by Sodupe *et al.*[43] obtained at the MCPF level of theory, however, no RCCSD(T) value was obtained here for this complex as the calculation exceeded the available resources.

The observation that the removal of a water molecule from $[Mg(H_2O)_2]^+$ requires less energy than from Mg^+–H_2O is also seen to be in agreement with the previous work.[32,43] This is opposite to the finding for $[Ca(H_2O)_2]^+$ (see Chapter 8), but in line with the rest of the results on Ca^+, and those in the current study, in that the removal of a ligand from [Y–Mg–X]$^+$ (where Y and X = H_2O, CO_2 and N_2) is smaller than the removal of the same ligand from Mg^+-X (where X = H_2O, CO_2 and N_2). However, with [Y–Mg–X]$^+$ (where Y=O or O_2 and X= H_2O, CO_2 and N_2) the energy for removal of the closed shell ligand is significantly higher than that from Mg^+-X where X = H_2O, CO_2 and N_2), in line with the formal Mg^{2+} in these complexes.

9.5 Conclusions

Optimized geometries and vibrational frequencies have been obtained for a range of Mg^+ containing complexes which are thought to be of importance in the chemistry of magnesium in the MLT region of the

Earth's atmosphere. For the Mg^+–L complexes, there was a general agreement with previous experimental and theoretical results, where available. There were discrepancies with some values, in particular for Mg^+–O_3. However, owing to the level of theory, the expected trend for MgO^+, MgO_2^+ and MgO_3^+, and the general agreement with experiment and the previous highest levels of calculations in this work, suggests that the previously reported[14] low value for $D_0[Mg^+–O_3]$ is in error, as is a very low value for $D_0[Mg^+–O_2]$.[46]

Table 9.9. Binding Energies, D_0 (D_e) for X–Mg+–Y complexes (kJ mol^{-1}).

	Removal of X		Removal of Y	
Species	B3LYP	RCCSD(T)	B3LYP	RCCSD(T)
H_2O—Mg^+— CO_2	108.3 (116.3)	112.3 (120.1)	39.4 (42.6)	48.5 (51.7)
N_2—Mg^+—CO_2	16.5 (19.5)	22.2 (25.1)	50.1 (52.0)	59.2 (61.1)
N_2—Mg^+—H_2O	14.1 (17.6)	19.5 (23.0)	116.6 (123.8)	120.2 (127.5)
N_2—Mg^+—O_2	96.1 (100.9)	96.1 (100.9)	118.8 (125.0)	156.1 (162.2)
N_2—Mg^+—O	85.9 (90.6)	91.2 (95.8)	266.1 (272.4)	277.3 (283.6)
O_2—Mg^+—H_2O	138.8 (145.4)	173.1 (179.7)	218.5 (227.5)	213.8 (222.8)
O—Mg^+—CO_2	278.3 (284.2)	288.9 (294.8)	131.6 (134.9)	139.7 (143.0)
O—Mg^+—H_2O	285.0 (291.7)	293.2 (299.9)	207.3 (216.1)	207.8 (216.6)
O_2—Mg^+—CO_2	130.8 (136.5)	167.2 (173.0)	141.5 (145.0)	144.2 (147.7)
O_2—Mg^+—O	124.5 (127.5)	66.4 (69.4)	282.0 (285.3)	192.6 (195.9)
N_2—Mg^+—N_2	22.0 (24.8)	27.8 (30.6)		
O_2—Mg^+—O_2	73.5 (75.4)	71.2 (73.1)		
CO_2—Mg^+—CO_2	42.3 (44.6)	___[a]		
H_2O—Mg^+—H_2O	101.3 (109.5)	105.3 (113.5)		

[a] exceeds resources.

Energies for removal of each ligand from $[Y–Mg–X]^+$ complexes have also been calculated, after the global minima was established. For the species which have Y = O or O_2 as a ligand it can be observed that the binding energy of the second ligand, X, is greater than in the Mg^+–X complex, owing to the higher formal charge on the magnesium atom.

In line with previous work, it is found the diligated complexes, where the ligand is H_2O, CO_2 or N_2, prefer to have the two ligands approaching from the same side, in contrast to the case for the calcium-containing complexes (see Chapter 8). This is in line with results obtained for $[MgX_2]^+$ and $[CaX_2]^+$ complexes, where *sp* hybridization in the magnesium species leads to the same side being preferred for the two ligands, whereas *sdσ* hybridization leads to different sides being preferred in the case of calcium. Interestingly, for the corresponding dications, $[MgX_2]^{2+}$, approach from different sides is favoured (as sp^2 hybridization cannot occur),[35,43] and this is consistent with the results we find for the $[O–Mg–Y]^+$ and $[O_2–Mg–Y]^+$ complexes, where the magnesium is formally doubly-charged.

The results of the calculations reported here are going to be used in modelling laboratory studies of many of these reactions, for later inclusion in a new atmospheric model of magnesium.[48]

References

[1] J. M. C. Plane and M. Helmer, *Faraday Discuss.* 1995, **100**, 411.

[2] , G. J. Molina-Cuberos, H. Lammer, W. Stumptner, K. Schwingenshuh, H. O. Rucker, J. J. López-Moreno, R. Rodrigo and T. Tokano, *Planet. Space Sci.* 2001, **49**, 143.

[3] R. J. Plowright, T. G. Wright and J. M. C Plane, *J. Phys. Chem. A,* 2008, **112**, 6550.

[4] S. E. Daire, J. M. C. Plane, S. D. Gamblin, P. Soldán, E. P. F. Lee and T. G. Wright, *J. Atmos. Sol.-Terr. Phys.,* 2002, **64**, 863.

[5] J. M. C. Plane, R. J. Plowright and T. G. Wright, *J. Phys. Chem. A,* 2006, **110**, 3093.

[6] W. Swider, *Planet. Space. Sci.,* 1984, **32***,* 307.

[7] E. Kopp, P. Eberhardt, U. Hermann and L. G. Bjorn, *J. Geophys. Res.*, 1985, **90**, 13041.

[8] U. von Zahn, R. A. Goldberg, J. Stegman and G. Witt, *Planet. Space. Sci.,* 1989, **37**,657.

[9] J. G. Anderson and C. A. Barth, *J. Geophys. Res.,* 1971, **76**, 3723.

[10] J. -C. Gerard and A. J. Monfils, *Geophys. Res.,* 1974, **79,** 2544.

[11] T. Vondrak, J. M. C. Plane, S. Broadley and D. Janches, *Atmos. Chem. Phys.,* 2008, **8**, 7015.

[12] S. C. Collins, J. M. C. Plane, M. C. Kelley, T. G. Wright, P. Soldan, T. J. Kane, A. J. Gerrard, B. W Grime, R. J Rollason, J. S. Friedman, S. A. Gonzalez, Q H. Zhou, M. P. Sulzer and C. A. Tepley, *J. Atmos. Sol.-Terr. Phys.* 2002, **64**, 845.

[13] *Meteors in the Earth's Atmosphere;* E. Murad, I. W. Williams., Eds, Cambridge University Press, Cambridge, 2002

[14] S. Petrie, *Env. Chem.,* 2005, **2**, 308.

[15] S. Petrie and R. C. Dunbar, *Astrochemistry: From Laboratory Studies to Astronomical Observations*, *AIP Conf. Proc.,* 2006, **855**, 272.

[16] J. Frizenwallner and E. Kopp, *Adv. Space. Res.,* 1998, **21**, 859.

[17] S. Petrie and R. C. Dunbar, *J. Phys. Chem. A*, 2000, **104**, 4480.

[18] S. Petrie, *Env. Chem.* 2005, **2**, 25.

[19] K. R. S Woodcock, T. Vondrak, S. R. Meech and J. M. C. Plane, *Phys. Chem. Chem. Phys.*, 2006, **8**(15), 1812-1821.

[20] E. E. Ferguson, B. P. Rowe, D.W. Fahey and F. C. Fehsenfeld, *Planet. Space Sci.,* 1981, **29**, 479.

[21] B. J. Murray and J. M. C. Plane *Atmos. Chem. and Phys.*, 2005, **5**, 1027-1038.

[22] Gaussian 03, Revision C.02, [22] M. J. Frisch, G. W. Trucks, H. B. Schlegel, G. E. Scuseria, M. A. Robb, J. R. Cheeseman, J. A. Montgomery, Jr., T. Vreven, K. N. Kudin, J. C. Burant, J. M. Millam, S. S. Iyengar, J. Tomasi, V. Barone, B. Mennucci, M. Cossi, G. Scalmani, N. Rega, G. A. Petersson, H. Nakatsuji, M. Hada, M. Ehara, K. Toyota, R. Fukuda, J. Hasegawa, M. Ishida, T. Nakajima, Y. Honda, O. Kitao, H. Nakai, M. Klene, X. Li, J. E. Knox, H. P. Hratchian, J. B. Cross, V. Bakken, C. Adamo, J. Jaramillo, R. Gomperts, R. E. Stratmann, O. Yazyev, A. J. Austin, R. Cammi, C. Pomelli, J. Ochterski, P. Y. Ayala, K. Morokuma, G. A. Voth, P. Salvador, J. J. Dannenberg, V. G. Zakrzewski, S. Dapprich, A. D. Daniels, M. C. Strain, O. Farkas, D. K. Malick, A. D. Rabuck, K. Raghavachari, J. B. Foresman, J. V. Ortiz, Q. Cui, A. G. Baboul, S.Clifford, J. Cioslowski, B. B. Stefanov, G. Liu, A. Liashenko, P. Piskorz, I. Komaromi, R. L. Martin, D. J. Fox, T. Keith, M. A. Al-Laham, C. Y. Peng, A. Nanayakkara, M. Challacombe, P. M. W. Gill, B. G. Johnson, W. Chen, M. W. Wong, C. Gonzalez and J. A. Pople Gaussian, Inc., Wallingford CT, 2004.

[23] MOLPRO is a package of *ab initio* programs written by H. J. Warner, P. J. Knowles and others.

[24] J. W. Ochterski, G. A. Petersson and J. A. Montgomery Jr., *J. Chem. Phys.,* 1996, **104**, 2598.

[25] L. Operti, E. C. Tews,T. J. MacMahon and B. S. Freiser, *J. Am. Chem. Soc.*, 1989 **111**, 9152.

[26] C. S. Yeh, K. F. Willey, D. L. Robbins, J. S. Pilgrim and M. A. Duncan, *Chem. Phys. Lett*, 1992, **196**, 233.

[27] K. F. Willey, C. S. Yeh, D. L. Robbins, J. S. Pilgrim and M. A. Duncan, *J. Chem. Phys.,* 1992, **97**, 8886.

[28] M. A. Duncan, *Annu. Rev. Phys. Chem.,* 1997, **48**, 69.

[29] F. Misaizu, M. Sanekata, K. Tsukamoto, K. Fuke and S. Iwata, *J. Phys. Chem.,* 1992, **96**, 8259.

[30] K. Fuke, F. Misaizu, M. Sanekata, K. Tsukamoto and S. Iwata, *Z. Physik D* 1993, **26**, S180.

[31] F. Misaizu, M. Sanekata, K. Fuke and S. Iwata, *J. Chem. Phys.,* 1994, **100**, 1161.

[32] H. Watanabe, S. Iwata, K. Hashimoto, F. Misaizu and K. Fuke, *J. Am. Chem. Soc.,* 1995, **117**, 755.

[33] H. Watanabe and S. Iwata, *J. Chem. Phys.,* 1998, **108**, 10078.

[34] C. W. Bauschlicher Jr. and H. Partridge, *J. Phys. Chem.,* 1991, **95**, 3946.

[35] C. W. Bauschlicher Jr, M. Sodupe and H. Partridge, *J. Chem. Phys.*, 1992, **96**(6), 4453.

[36] M. Sodupe and C. W. Bauschlicher, Jr., *Chem. Phys. Lett.,* 1992, **195**, 494.

[37] A. Andersen, F. Muntean, D. Walter, C. Rue and P. B. Armentrout, *J. Phys. Chem. A,* 2000, **104**, 692.

[38] R. C. Dunbar and S. Petrie *J. Phys. Chem. A,* 2005, **109**, 1411.

[39] H. Tachikawa and H. Yoshida, *J. Mol. Struct.(Theochem),*1996, **363**, 263.

[40] P. Maitre, C. W. Bauschlicher and H. Partridge, *Chem. Phys. Lett.,* 1994 **225**, 467.

[41] D. L. Robbins, L. R Brock, J. S. Pilgrim and M. A Duncan, *J .Chem. Phys.*, 1995, **102**, 1481.

[42] K. F. Willey, C. S. Yeh, D. L. Robbins and M. A. Duncan, *Chem. Phys. Lett*, 1992, **192**, 179.

[43] M. Sodupe, C. W. Bauschlicher Jr. and H. Partridge, *Chem. Phys. Lett.* 1992, **192**, 185.

[44] C. W. Bauschlicher Jr., S. R. Langhoff and H. Partridge, *J. Chem. Phys.*,1994 **101**(3), 2644.

[45] H. Partridge, S. R. Langhoff and C. W. Bauschlicher, Jr., *J. Chem. Phys.,* 1986, **84**, 4486.

[46] B. S. Jursic, *J. Molec. Struct. (THEOCHEM)*, 2000, **530**, 59.

[47] M. M. Kappes and R. H. Staley, *J. Phys. Chem.*, 1981, **85**, 942

[48] C. L. Whicker, J. C. Gomez Martin, T. G. Wright and J. M. C. Plane to be submitted.

[49] B. R. Rowe, D. W. Fahey, E. E. Ferguson and F. C. Fehsenfeld, *J. Chem. Phys.,* 1981, **75**, 3325.

[50] N. F. Dalleska, and P. B. Armentrout, *Int. J. Mass Spectrom. Ion Process*, 1994 **134** (2-3), 203.

[51] M. Sodupe and C. W. Bauschlicher Jr., *Chem. Phys. Lett.* 1993, **203**, 215.

[52] J. Chen, T. H. Wong and P. D. Kleiber, *J. Chem. Phys.*, 1998, **109**(19), 8311.

[53] *Gas-Phase Ion and Neutral Thermochemistry*, S. G. Lias, J. E. Bartmess, J. F. Liebman, J. L. Holmes, R. D. Levin and W. G. Mallard, *J. Phys. Chem. Reference Data* 1988, ***17***, Suppl. 1. (AIP, New York, 1988).

[54] S. L. Broadley, T. Vondrak and J. M. C. Plane, *Phys. Chem. Chem. Phys.* 2007, **9**, 4357.